THE JOURNAL OF BIOLOGICAL CHEMISTRY VOL. 282, NO. 32, pp. 23316–23325, August 10, 2007

Effect of Calcium on Calmodulin Bound to the IQ Motifs of Myosin V*[S]

Received for publication, February 23, 2007, and in revised form, June 4, 2007 Published, JBC Papers in Press, June 11, 2007, DOI 10.1074/jbc.M701636200

Kathleen M. Trybus[‡1], Marina I. Gushchin[‡], HongJun Lui[§], Larnele Hazelwood[§], Elena B. Krementsova[‡], Niels Volkmann[§2], and Dorit Hanein[§]

From the [‡]Department of Molecular Physiology and Biophysics, University of Vermont, Burlington, Vermont 05405 and [§]The Program of Cell Adhesion, Burnham Institute for Medical Research, La Jolla, California 92037

The long neck of unconventional myosin V is composed of six tandem "IQ motifs," which are fully occupied by calmodulin (CaM) in the absence of calcium. Calcium regulates the activity, the folded-to-extended conformational transition, and the processive run length of myosin V, and thus, it is important to understand how calcium affects CaM binding to the IQ motifs. Here we used electron cryomicroscopy together with computer-based docking of crystal structures into three-dimensional reconstructions of actin decorated with a motor domain-two IQ complex to provide an atomic model of myosin V in the presence of calcium. Calcium causes a major rearrangement of the bound CaMs, dissociation of CaM bound to IQ motif 2, and propagated changes in the motor domain. Tryptophan fluorescence spectroscopy showed that calcium-CaM binds to IQ motifs 1, 3, and 5 in a different conformation than apoCaM. Proteolytic cleavage was consistent with CaM preferentially dissociating from the second IQ motif. The enzymatic and mechanical functions of myosin V can, therefore, be modulated both by calcium-dependent conformational changes of bound CaM as well as by CaM dissociation.

Myosin V is a double-headed, processive motor involved in transport of organelles, mRNA, and membrane trafficking (for review, see Ref. 1). A striking feature of this motor is its elongated neck region that is composed of six IQ motifs (consensus sequence IQ*XXX*R*G**XXX*R, where *X* is any amino acid), each of which binds CaM[3] or a CaM-like light chain. The long neck region enables myosin V to take 36-nm steps on actin as it moves in a hand-over-hand fashion, with communication between the heads coordinated via a strain-dependent mechanism (for reviews, see Refs. 2 and 3). In addition to its mechanical role, the neck is also involved in regulating myosin V function. In the absence of calcium, all six of the IQ motifs of murine myosin V bind apoCaM (4). Myosin V adopts a folded, inactive conformation under these conditions provided that cargo is not present (5–9). Low calcium concentrations or cargo binding in the absence of calcium unfold and activate the molecule, whereas higher calcium concentrations inhibit motility and processive movement by dissociating CaM from one or more of the IQ motifs (5, 10, 11).

It is important to know the structure of CaM bound to the IQ motifs in both the apo- and in the calcium-saturated states to fully understand how the neck functions. We have previously developed atomic models for a myosin V motor domain-two IQ complex bound to actin in the absence of calcium and in several nucleotide states that mimic the progression through the ATPase cycle (12). The key results from that study were 1) ATP opens the long cleft dividing the motor domain, providing a mechanism by which the strong binding actomyosin interface is disrupted, 2) loop 2 at the actin interface is rearranged to act as a tether, when myosin is in the weak binding states, and 3) a pre-powerstroke transition state bound to actin was visualized for the first time through the use of nucleotide analogs and improved computational methods. The actin-bound MD-2IQ in the absence of calcium and nucleotide from our previous study (12) was used for comparison with the results presented here in the presence of calcium.

A high resolution crystal structure of apoCaM bound to the first two IQ motifs of murine myosin V was also solved recently, which serves as a model for the entire neck of mammalian myosin V (13). It was unclear how apoCaM could bind an IQ motif, because unbound apoCaM exists with both the N-lobe and the C-lobe in a closed, non-gripping conformation. Calcium binding opens both lobes, allowing CaM to adopt a gripping conformation, which is the typical way that CaM binds to and activates a target peptide (14–16). The crystal structure revealed that apoCaM adopts a new conformation when bound to the IQ motifs. The C-terminal lobe of each CaM adopts a semi-open conformation that grips the first part of the IQ motif (IQ*XXX*R; *X* indicates any amino acid), whereas the N-terminal lobe adopts a closed conformation that interacts more weakly with the second part of the motif (G*XXX*R). A surprising finding was the pivotal role played by the non-consensus residues in the IQ motif, which determine the precise structure of the bound CaM. Each IQ motif is, thus, expected to display some unique

* This work was supported by National Institutes of Health Grants HL38113 (to K. M. T.), AR47199 (for electron microscopy, to D. H.), and GM076503 (for software development, to N. V.). The costs of publication of this article were defrayed in part by the payment of page charges. This article must therefore be hereby marked "*advertisement*" in accordance with 18 U.S.C. Section 1734 solely to indicate this fact.

[S] The on-line version of this article (available at http://www.jbc.org) contains supplemental Movies 1 and 2.

[1] To whom correspondence may be addressed: Dept. of Molecular Physiology and Biophysics, University of Vermont, 149 Beaumont Ave, Burlington, VT 05405. Tel.: 802-656-8750; Fax: 802-656-0747; E-mail: kathleen.trybus@uvm.edu.

[2] To whom correspondence and requests for coordinates may be addressed. Tel.: 858-646-3187; Fax: 858-646-3195; E-mail: niels@burnham.org.

[3] The abbreviations used are: CaM, calmodulin; AVID, absolute values of individual differences; IHRSR, iterative helical real space refinement; MD, motor domain; MD-2IQ, complex containing the motor domain and the adjacent two IQ motifs of murine myosin V; GST, glutathione *S*-transferase.

interactions with apoCaM, although the overall lobe conformation (semi-open C-lobe, closed N-lobe) remains the same.

There has been no structural information to show how calcium affects the binding of CaM to the IQ motifs of myosin V. Here we use electron cryomicroscopy to show that calcium causes the lever arm of actin-bound myosin V to adopt a conformation distinct from that observed when apoCaM is bound to the IQ motifs of myosin V as well as causing propagated changes in the motor domain. Results from fluorescence spectroscopy also show that calcium-CaM bound to an IQ motif peptide adopts a different conformation from bound apoCaM. Microscopy and solution studies implicate IQ motif 2 as the site from which CaM dissociates in the presence of calcium. Calcium, thus, exerts its effect on myosin V function both by changing the conformation of bound CaM as well as by causing CaM dissociation.

MATERIALS AND METHODS

Protein Preparation—The murine myosin V construct consisting of the motor domain and two CaM binding IQ motifs (MD-2IQ) was truncated at amino acid 820 followed by a C-terminal FLAG epitope (DYKDDDDK) for purification by affinity chromatography. A similar construct containing one IQ motif (MD-1IQ) was truncated at amino acid 795. This construct was used for image processing to get an independent boundary between the two IQ motifs. Three mutant MD-2IQ constructs were also produced. In each of these, the wild-type DNA sequence at the second IQ motif after the motor domain was replaced by the sequence from the first, fourth, or sixth IQ motif of the wild-type molecule. Protein expression in Sf9 cells and purification is described in Krementsov *et al.* (5). Chicken skeletal muscle actin was prepared and stored as described (17).

Adjacent pairs of IQ motifs derived by PCR from the heavy chain of murine myosin V were cloned into pGEX-2T (Amersham Biosciences), creating a fusion protein containing glutathione *S*-transferase (GST) at the N terminus followed by a thrombin cleavage site. The 1–2 IQ motif pair corresponds to amino acids 765–820 of the murine myosin V heavy chain, the 3–4 IQ pair to amino acids 813–867, and the 5–6 IQ pair to amino acids 861–908. CaM was cloned into a modified kanamycin-resistant vector (T7 RNA polymerase promoter, p15A origin of replication). The CaM-containing vector (kanamycin-resistant) and the IQ-containing pGEX-2T vector (ampicillin-resistant) were co-transformed into the *Escherichia coli* BL21 (DE3) strain and grown on LB plates containing both antibiotics. Cultures were grown overnight at 37 °C in enriched media (20 g/liter Tryptone, 10 g/liter yeast extract, 5 g/liter NaCl, 2 ml/liter glycerol, and 50 mM potassium phosphate, pH 7.2). The cells were disrupted by sonication. The clarified supernatant was incubated with glutathione-Sepharose 4B affinity matrix for 1 h at 4 °C. The resin-protein mixture was then poured into a column and washed with phosphate-buffered saline. The GST fusion protein was eluted with glutathione (0.154 g of reduced glutathione dissolved in 50 ml of 50 mM Tris-HCl, pH 8.0). The GST was removed by thrombin cleavage (10 units/mg of IQ-CaM complex) followed by a second glutathione-Sepharose 4B affinity column to remove the liberated GST.

Electron Microscopy of Actomyosin V Complexes—F-actin was diluted to 30–50 μg/ml with 20 mM NaCl, 5 mM sodium phosphate, pH 7.0, 1 mM $MgCl_2$, 0.1 mM EGTA, 3 mM NaN_3 just before application to the glow-discharged 400-mesh copper grids coated with holey carbon film. After a 1-min incubation in a humid chamber, the grids were rinsed twice with 10 mM imidazole, pH 7.0, 10 mM NaCl, 1 mM EGTA, 1.5 mM $CaCl_2$, 1 mM $MgCl_2$, 1 mM dithiothreitol, 3 mM NaN_3 (dilution buffer). The myosin sample was preincubated for 30 min on ice in dilution buffer. The myosin sample, diluted to ≈0.1 mg/ml in dilution buffer, was applied to the grid for 30 s and replaced by an additional drop of sample (30 s). Excess liquid was blotted off, and the grids were plunged into liquid ethane cooled by liquid N_2.

Low-dose images were recorded with a Tecnai G2 T12 electron microscope (FEI Electron Optics, The Netherlands) equipped with a LaB_6 filament and a DH626 cryo-holder (Gatan, Pleasaton, CA) at a nominal magnification of 52,000× using 120 keV and a 1.5-μm defocus and with total electron dose of 10 $e^-/Å^2$. Micrographs were digitized with a SCAI scanner (Integraph, Phoenix, AZ) with a pixel size of 0.27 nm on the sample.

Reconstruction Procedures—Helical reconstructions were obtained for all data sets with the Brandeis Helical Package (18) as described (17). All reconstructions included 23 layer lines that were trimmed to 2.1-nm resolution. Because this resolution is within the first zero of the contrast transfer function, no phase correction was necessary. The abrupt edge that was introduced by this procedure was smoothed to zero by using a Gaussian falloff. Only layer lines that were found to be statistically significant in at least one of the individual filaments were used and included orders 2, −11, 4, −9, 6, −7, 8, −5, −3, −1, −12, 3, 14, 1, 5, −8, −4, −2, 7, −6, 13, and the equator. Individual filaments were reconstructed separately, aligned in real space (17, 19), normalized, and averaged. The independent far and near side maps were kept separate and used for cross- validation.

The iterative helical real space refinement (IHRSR) method (20) is a hybrid approach that uses real-space, single-particle processing and imposition of helical symmetry in an iterative manner. Our implementation uses EMAN (21) for the single-particle reconstruction portion and routines adapted from the CoAn suite (22, 23) to determine and impose the helical symmetry. A box size of 80 × 80 pixels with a 0.54 nm pixel size was used. This corresponds to about 15 asymmetric units of the helix, a little more than one actin crossover. An overlap of 60 pixels was chosen, allowing every asymmetric unit to contribute to four different views of the helix. To generate independent IHRSR reconstructions for cross-validation, the data were split into two random halves which where independently reconstructed.

Docking and Modeling—At least two independently derived maps were used to cross-validate all docking, modeling, and segmentation results. An atomic model for filamentous actin, based on rigid-body refinement against fiber diffraction data (24) followed by refinement against constraints from electron microscopy and cross-linking studies (12), was docked into maps of undecorated actin. After real-space alignment (25), the reconstruction of undecorated actin was subtracted from the

respective myosin V-decorated maps. Single units of the actin-bound myosin V densities were isolated with the watershed transform segmentation program (26). The resulting densities, due only to myosin V, were further subsegmented to delineate the densities for the motor domain (MD) and the CaMs. This was done to ensure that the refined positions of the CaM models are confined to the respective density unit and that they are not biased toward the higher density in the neighboring density unit. The boundary between the two CaMs was independently cross-validated by difference mapping of the MD-2IQ reconstruction with a reconstruction of an construct that lacked the second IQ motif (MD-1IQ, data not shown).

Statistics-based modular docking (22, 23) was used throughout to build models of the actin-bound myosin V. The structure was divided into the motor domain and the two CaM regions (IQ1 and IQ2). For the MD docking the available structures were divided into three groups. The post-power-stroke conformation was represented by PDB codes 1mma, 1mmn, 1mmd, 1mmg, 2mys, 1kk7, 1fmv, 1fmw, and 1w7j. The pre-power-stroke conformation was represented by PDB codes 1br1, 1br2, 1br4, 1dfl, 1mnd, and 1vom. The third group contains the myosin V crystal structures with a similar lever-arm position as the post-stroke conformation but a more tightly closed actin binding cleft in the absence of nucleotide; PDB codes 1oe9, 1w8j (four asymmetric units), and 1w7i. There was no significant difference ($p < 0.001$) between the first and the third group, implying that we cannot pick up the cleft state by docking alone, but the fit of the second group was significantly worse than for the other two groups. Modeling was continued using the docked 1oe9 coordinates.

The two bound CaMs were modeled using the CaM-like essential light chain (LC1-sa) taken from the myosin V crystal structure. Docking was done into discrepancy maps that had the MD portion removed. The resulting MD/CaM boundary was very similar to that determined by segmentation. The initial placement of the first CaM was extrapolated from the docked crystal structure and then refined using the refinement module from CoAn. After docking, the contribution of the first CaM model was removed from the map by discrepancy mapping, and then the second CaM model was docked into the remainder without constraints. The discrepancy boundary was again very similar to the one determined independently by difference mapping and segmentation. Regularization with REFMAC5 (27) was performed for all atomic models to relieve distortions in stereochemistry.

Discrepancy, Difference, and Structural Flexibility Mapping—For "discrepancy mapping," density is first calculated from the docked atomic model using electronic scattering factors. Then image-formation and image-analysis artifacts present in the reconstruction are compensated for by matching the Fourier amplitude spectrum of the calculated density to that observed and by scaling the densities appropriately. Last, the modified density is subtracted voxel-wise from the observed reconstruction. The resulting discrepancy maps allow reliable localization of regions where the reconstruction has significantly more density than the model can explain. Through the use of multiple maps and crystal structures, an error estimate (S.D.) for each voxel in the discrepancy maps can be calculated. This feature allows assignment of statistical significance. Peaks were considered significant if their value was at least three times their S.D. The results were cross-validated between the helical reconstructions and the IHRSR maps.

"Difference mapping" and error assessment were carried out using the real space averages and variances for helical reconstructions. Difference maps for the IHRSR maps were calculated without error assessment. Before subtracting, the helical reconstructions were aligned to each other using a hybrid real space reciprocal space alignment procedure that includes common features of the two maps in the alignment (19); alignment involving IHRSR maps was done using real-space correlation (22, 23). For difference maps between helical reconstructions, we tested the significance of each difference between corresponding pairs of real space voxels using a classic t test at a confidence level of 99.9% ($p < 0.001$). Difference maps between different IHRSR maps and between IHRSR maps and helical maps were used for cross-validation. Only differences that were consistently present (and significant at 99.9% were applicable) were used for interpretation.

Absolute values of individual differences (AVID) was used to map intensity variations of individual actomyosin units within filaments (28). These variations can either be caused by partial occupancy or by a mixture of conformations. Because the AVID procedure excludes the layer line data used for helical reconstruction, the resulting AVID map contains data that is independent of the data used for the three-dimensional reconstruction and difference mapping. Four AVID maps were generated of myosin V in the presence (two maps) and absence of calcium (two maps). Only peaks present in the two AVID maps of myosin V in the presence of calcium and not in the AVID maps of myosin V in the absence of calcium were considered for interpretation as effects of calcium addition.

Fluorescence Spectroscopy—Fluorescence measurements were performed on an ISS Inc. spectrofluorometer (Model ISS K2; Champaign, IL) equipped with a 300-watt xenon arc lamp as an excitation source and a temperature controlled cell-housing (20 °C). Tryptophan fluorescence of the CaM-IQ complexes was excited at 290 nm, and the emission spectra were collected from 300 to 400 nm with a 320-nm cutoff filter in the emission path. The spectral bandwidths were 8 nm for excitation and 8 nm for emission. Emission spectra were recorded in ratio mode. Buffers contained final concentrations of either 1 mM EGTA or 1 mM EGTA and 1.5 mM $CaCl_2$.

Acrylamide Quenching of Trp Fluorescence—Acrylamide quenching was used to determine the degree of exposure of the single tryptophan residue present in each IQ-CaM complex. The decrease in fluorescence intensity at the wavelength maximum was measured as a function of increasing acrylamide concentration. The fluorescence intensity in the absence of quencher (F_0) divided by the fluorescence intensity in the presence of quencher (F) was used to quantify the change in fluorescence resulting from acrylamide quenching (F_0/F). F_0/F was plotted as a function of acrylamide concentration, [Q], and fit to the Stern-Volmer relationship taking into account both static (V) and dynamic quenching (K_{SV}) constants: $F_0/F = (1 + K_{SV}[Q])(\exp V[Q])$ (29). Buffers contained final concentrations of either 1 mM EGTA or 1 mM EGTA and 1.5 mM $CaCl_2$.

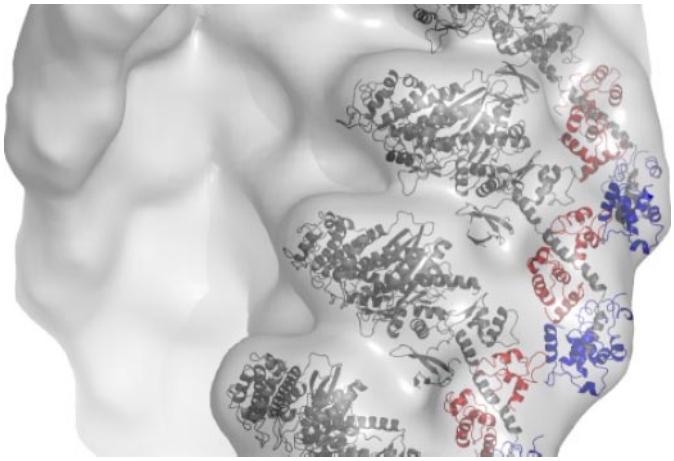

FIGURE 1. **Three-dimensional reconstruction of actin filaments decorated with a myosin V-2IQ construct in the presence of calcium.** The final model and the corresponding three-dimensional reconstructions are shown for several adjacent MD-2IQ molecules. Docked myosin structures are shown in schematic representation, with the motor domain in *gray* and the two CaM molecules in *red* and *blue*. The pointed end of the actin filament is at the *top* of the figure. Comparable data in the absence of calcium were previously published in Volkmann *et al.* (12).

Thrombin Cleavage—CaM-IQ complexes (0.4 mg/ml in 10 mM HEPES, pH 7.2, 10 mM NaCl, 3 mM $CaCl_2$) were cleaved with human α-thrombin at 10 units/mg of complex (Hematologic Technologies Inc.) for 5 h at 37 °C. The proteolytic products were analyzed on a 15% SDS-PAGE gel. The wild-type and mutant MD-2IQ complexes (0.5 mg/ml in 10 mM HEPES, pH 7.8, 150 mM NaCl, 1 mM dithiothreitol, 37 °C with either 0.4 mM $CaCl_2$ or 1 mM EGTA) were similarly cleaved with 10 units of thrombin/mg protein and analyzed on 6.5% SDS-polyacrylamide gels.

RESULTS

Atomic Model of Myosin V Bound to Actin in the Presence of Calcium—Electron cryomicroscopy and helical reconstruction techniques were used to generate three-dimensional maps for a myosin V motor domain-2IQ (MD-2IQ) construct bound to actin in the presence of calcium and in the absence of nucleotide (Fig. 1). The comparable experiments done without calcium have been previously described and are used for comparison with the results described here (12). MD-2IQ contains the motor domain and the two IQ motifs adjacent to it together with bound CaM. The CaM molecules are sequentially numbered with respect to their position relative to the MD, with the first CaM adjacent to the MD. The data sets were first processed using standard helical reconstruction techniques. In contrast to the well defined density of the second CaM in the calcium-free actomyosin three-dimensional maps (12), the second CaM was difficult to resolve in the presence of calcium. Use of the iterative real space refinement method (20), a technique that includes classification procedures capable of sorting mixtures of actin-bound myosin conformations (12), was needed to resolve the second CaM. Even after sorting, the density for the second CaM is considerably less well defined than the one for the first CaM, but the definition is now good enough to model the CaM into the density (Fig. 1).

An atomic model was generated using a quantitative fitting procedure, based on existing crystal structures (see "Materials and Methods"). The same approach was previously used to generate a model for actin-bound MD-2IQ in the absence of calcium (12). There are no significant differences in the docked orientation and position of the actin-bound motor domain when compared with the calcium-free state, but the CaMs do move substantially (see below).

Calcium-dependent Changes in the Motor Domain—To analyze changes upon the addition of calcium, we calculated four types of maps in the motor-domain region (see also "Materials and Methods"); (i) discrepancy maps, obtained by subtracting the density calculated for the atomic model from the density of the three-dimensional reconstruction (*magenta* in Fig. 2; this approach identifies regions of higher density in the reconstruction that are not accounted for by the atomic models), (ii) difference maps subtracting the density of the maps in the absence of calcium from the density in its presence (*yellow* in Fig. 2; these maps indicate strengthening of density features when calcium is added), (iii) difference maps subtracting the density of the maps in the presence of calcium from the density in the absence of calcium (*green* in Fig. 2; these maps indicate weakening of density upon addition of calcium), (iv) AVID maps, indicating either partial occupancy or structural flexibility (*blue* peaks in Fig. 2; this type of map was calculated in the entire map, including the IQ region).

Discrepancy mapping has been previously used to show whether the long cleft separating the upper and lower 50-kDa domains of the motor domain was closed or open in different nucleotide states in the actomyosin complex (12, 17, 30). In the absence of nucleotide, the long cleft of actin-bound MD-2IQ in the presence of calcium is closed to the same extent as was seen in the absence of calcium.

Loop 2, the ends of which are colored *blue* (Fig. 2*E*) shows the only discrepancy peak (Fig. 2, *A–C* and *E*, *magenta* density). This discrepancy peak is interpreted as showing that this region is stabilized upon binding to actin. Stabilization of loop 2 upon actin binding was previously reported for myosin V in the presence or absence of various nucleotides (12) as well as for smooth muscle and skeletal muscle myosin II (17, 30). A difference peak indicating higher density in the presence of calcium is close to loop 2 (*yellow peak* in Fig. 2*E*), indicating a shift of density in this region.

In the absence of calcium, there is a discrepancy peak also in the vicinity of loop 1 even when nucleotides are present (12). This peak, previously interpreted as stabilization of loop 1 (12), is missing in the presence of calcium (ends of loop 1 in *cyan* Fig. 2*H*). A difference peak indicating higher density in the absence of calcium (*green density* in Fig. 2*H*) is consistently located at the same position as the discrepancy peak of the calcium-free map. In addition, a difference peak indicating higher density in the presence of calcium (*yellow density* in Fig. 2*H*) resides at the back end of the upper 50-kDa domain. Thus, it appears that loop 1 is less well ordered in the presence of calcium and possibly attaches to a different site near the upper 50-kDa domain.

An AVID peak (*blue density* in Fig. 2) that is unique to the plus calcium state occurs at the SH3 domain located near the N terminus of myosin. The peak is adjacent to a difference peak, indicating higher density in this region in the absence of cal-

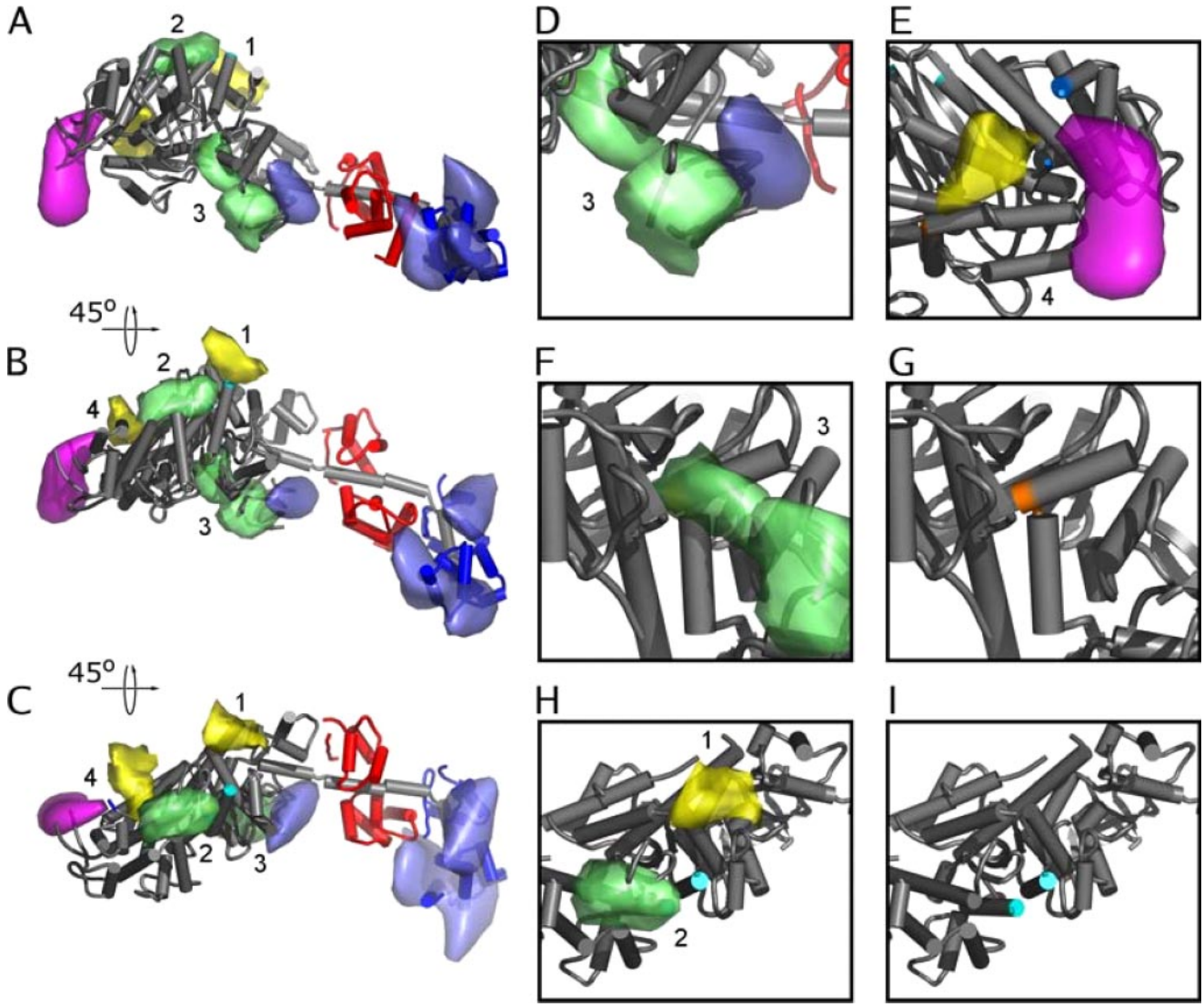

FIGURE 2. **Peak distribution mapped on the model for MD-2IQ in the presence of calcium.** *A–C*, overview. The actin filament would be to the *left* of the figure. In *A*, the pointed end of actin would be at the *top* of the figure. The motor domain is *gray*, and the two CaMs are in *red* and *blue*. For clarity, views rotated successively by 45° are also shown. The plus calcium discrepancy peak is shown in *magenta*; the AVID peaks unique to the plus calcium state are shown in *blue*. There is an additional AVID peak at the *top* of the upper 50-kDa domain that is common between the plus and minus calcium states (not shown). The differences between the two states are shown in *yellow* (higher density in the plus calcium state) and *green* (higher density in minus calcium state). Difference peaks are numbered to facilitate their identification in different orientations. All differences are statistically significant at a confidence level of 99.9%. *D*, enlarged SH3-like domain region showing the correlated difference and AVID peaks. *E*, close-up of the loop 2 region (ends shown in *blue*) showing the correspondence between the difference peak (*yellow*) and the discrepancy peak (*magenta*). This view is 180° around the *y* axis from *A*. *F–G*, close-up of the SH2 region. Cys-685 is colored in *orange*. *H–I*, close-up of loop 1 (ends *cyan*) region showing the two difference peaks.

cium (*green density* in Fig. 2). This combination of peaks (Fig. 2*D*) indicates that the SH3-like domain gets destabilized by the addition of calcium. Interestingly, the difference peak extends toward the SH2 helix and engulfs the sulfhydryl group (*orange* in Figs. 2, *F* and *G*), possibly indicating destabilization of this region in the presence of calcium.

Calcium-dependent Differences in the Lever Arm—In addition to these changes in the motor domain, calcium induces a significantly different conformation of the two CaMs adjacent to the motor domain (Fig. 3). Neither of the CaMs in the model of the actin-bound MD-2IQ in the absence of calcium (12) fit into the density obtained for the same actomyosin complex in the presence of calcium. The relative orientation of the CaM adjacent to the motor domain with respect to the lever arm helix had to be modified from that in the absence of calcium. The difference is not a simple movement of the lever arm up or down compared with the minus calcium state. It appears to be more of a shear-like motion where the first CaM tilts and slides up, whereas the second CaM tilts in a different direction and moves down. These motions are best illustrated in the two movies provided in supplemental data. The resolution is not, however, high enough to determine the exact lobe conformation of the CaMs.

A kink needed to be introduced in the lever arm between the two CaMs to allow both CaMs to occupy density. This operation also changes the relative orientation between the first and second CaMs when compared with the ~90° rotation around the relatively straight helix seen in the actin-bound state in the absence of calcium (12) or in the crystal structure of the two apoCaMs attached to IQ motifs 1 and 2 (13).

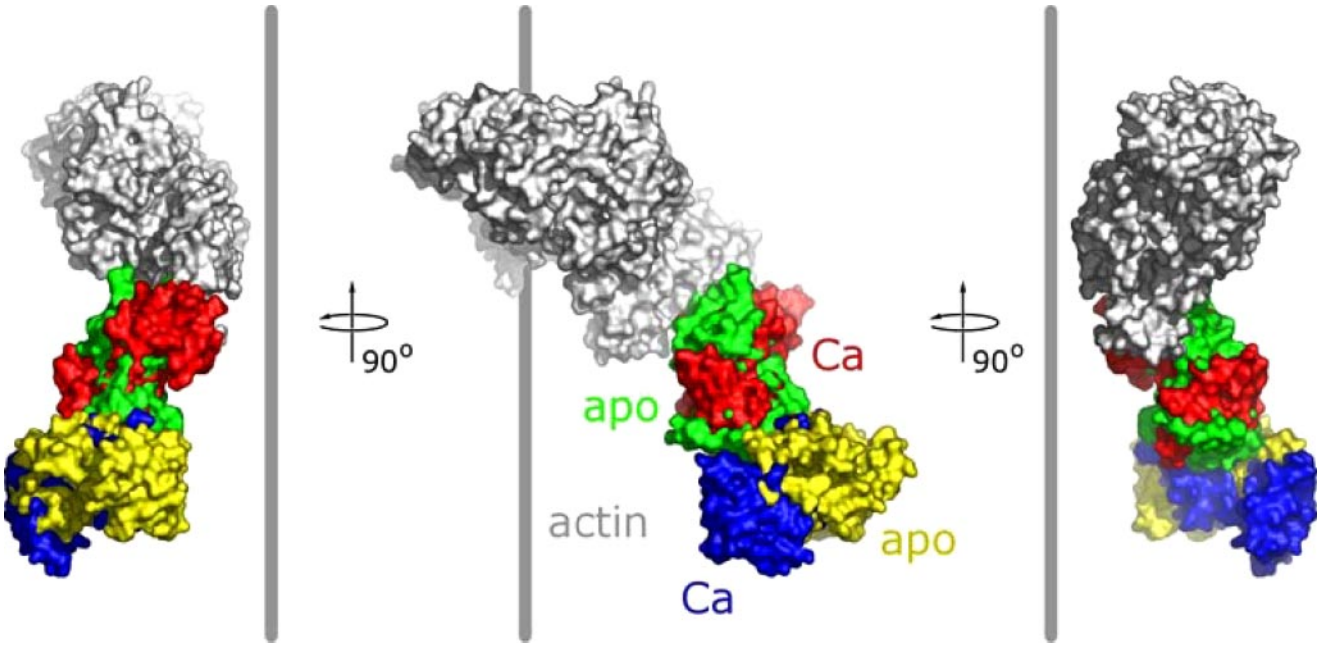

FIGURE 3. **Calcium affects the lever arm position.** Space-filling representation comparing the position of the two bound CaMs adjacent to the motor domain in the presence (*red*, *blue*) or absence (*green*, *yellow*) of calcium. The motor domain is shown in *gray*. The *three panels* are successively rotated by 90° around the actin axis (*gray line*). See the supplemental movies to view the conversion from the apoCaM to the calcium-CaM state from two angles to aid in interpretation of this figure.

For the actomyosin complex in the presence of calcium, a very large AVID peak was observed on the second CaM. The AVID procedure identifies mixtures of conformations or partial occupancy in helical reconstructions (28). Because the AVID peak encases a large part of the second CaM (*blue density* in Fig. 2), the most likely explanation for the AVID peak is that the second CaM has completely dissociated from some but not all of the MD-2IQ. This is further independently supported by the weak density in the three-dimensional reconstruction of the distal CaM in the presence of calcium and that sorting improves the definition of the density. If the weakening of the density would be caused by random disorder or structural variability, sorting would not lead to improvements. Neither an AVID peak nor weaker density in the distal CaM was observed for the same construct bound to actin in the absence of calcium (12). These observations support the idea that, in the presence of calcium, the second CaM is only bound in a subpopulation of the sample, whereas the rest is dissociated from the lever-arm helix.

Fluorescence Spectroscopy Shows Calcium-dependent Changes in CaM-IQ Motifs—Pairs of adjacent IQ motifs (1–2, 3–4, and 5–6) were co-expressed with CaM and purified as a complex (Fig. 4). CaM does not contain Trp residues, but each pair of IQ motifs contains a single Trp in the heavy chain of the odd-numbered IQ motifs of murine myosin V (Fig. 5). Fig. 5*B* illustrates the position of the Trp in IQ1 when apoCaM is bound. The maximum emission wavelength and the fluorescence intensity of the single Trp in each pair of IQ motifs will reveal if calcium causes its environment to change.

Fluorescence emission spectra were recorded from each of the complexes in the presence or absence of calcium and in the denatured state (Fig. 6). In all three complexes denaturation by 6 M guanidine HCl causes the tryptophan residue to be completely exposed to solvent, with a red-shifted emission maximum of ≈353 nm in the presence or absence of calcium. The maxima of the denatured spectra were normalized to one to facilitate comparison between complexes. In the native state, whether in the presence or absence of calcium, the maximum emission wavelength of each of the three complexes was significantly blue-shifted (327–334 nm) relative to the unbound state, indicating that in each case the Trp residue in the peptide was in a less solvent-exposed environment due to the bound CaM. These data provide strong evidence that CaM remains bound to IQ motifs 1, 3, and 5 both in the presence and absence of calcium.

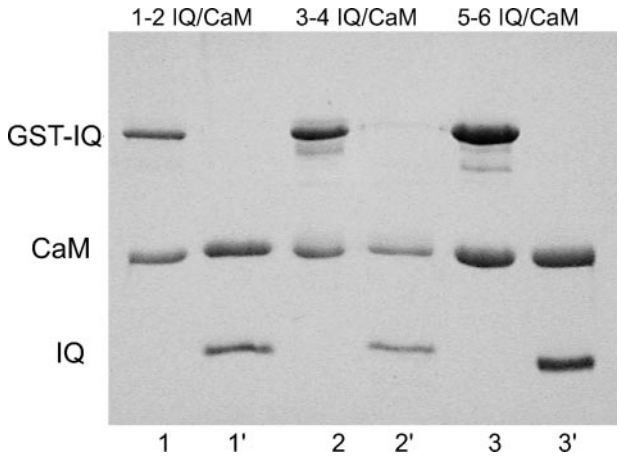

FIGURE 4. **Purification of CaM-IQ motif complexes.** CaM was co-expressed with a GST-IQ fusion protein containing either IQ motifs 1–2 (*lane 1*), motifs 3–4 (*lane 2*), or motifs 5–6 (*lane 3*). GST was removed by thrombin cleavage, resulting in a pure complex of a pair of IQ domains and bound CaM shown in *lanes 1′*, 2′, and 3′.

Each native complex, however, showed a different pattern of fluorescence change in response to calcium. For the 1–2 IQ-

A

		IQ	xxx	**RG**	xxx	**R**	
1st	KLRAACIR	**IQ**	KTI	**RG**	**W**LL	**R**	KRYL
2nd	CMQRAAIT	**VQ**	RYV	**RG**	YQA	**R**	CYAKFL
3rd	RRTKAATT	**IQ**	KY**W**	**RM**	YVV	**R**	RRYK
4th	IRRAATIV	**IQ**	SYL	**RG**	YLT	**R**	NRYRKI
5th	LREYKAVI	**IQ**	KRV	**RG**	**W**LA	**R**	THYK
6th	RTMKAIVY	**LQ**	CCF	**RR**	MMA	**K**	RELKKL

B

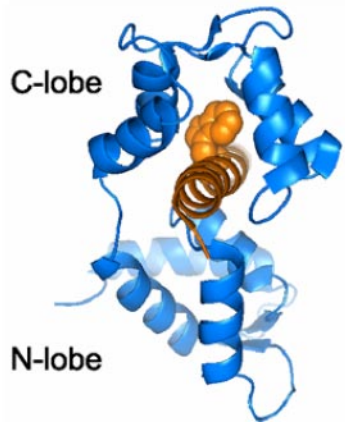

FIGURE 5. *A*, the amino acid sequence of the six IQ motifs of murine myosin V. Trp (W) in the first, third, and fifth IQ motif are *underlined*. The consensus IQ motif sequence is shown in the *top line*. Note that two amino acids in the sixth IQ motif differ from the published mouse myosin V sequence but by our sequencing are the same as in the chicken myosin V sequence (RDVKKL is actually RELKKL). *B*, location of the Trp residue in IQ motif 1 (*orange spheres*) when bound to apoCaM (PDB 1ix7). This is a key residue to anchor the semi-open C-lobe of apoCaM. The IQ motif is *orange*, and CaM is *blue*. The view is looking down from the motor domain.

CaM complex, calcium caused an ≈1.5-fold increase in fluorescence intensity and a small blue shift (334 to 327 nm), indicating that calcium caused the Trp residue to be in a less polar environment. The 5–6 IQ-CaM complex showed a 3-fold increase in fluorescence upon the addition of calcium but without an accompanying wavelength shift. In both the first and fifth IQ motif, the Trp residue is in position eight of the consensus sequence, following the conserved RG sequence (Fig. 5). In contrast, the 3–4 IQ-CaM complex has very high fluorescence relative to the denatured state in the absence of calcium, and calcium causes an ≈25% decrease in intensity without a change in the maximum emission wavelength. In the third IQ motif, Trp is in position five of the consensus sequence preceding the conserved residues RG, which may account for the different pattern.

Acrylamide Quenching—Acrylamide quenching was used to quantitatively assess the accessibility of the single Trp residue to solvent in the presence or absence of calcium. The Stern-Volmer relationship was used to fit the data and obtain the dynamic quenching constant, K_{SV} (Table 1). For both the 1–2 IQ-CaM and the 5–6 IQ-CaM complexes, the Trp residue was less accessible for quenching in the presence of calcium (Table 1). This result agrees qualitatively with the Trp fluorescence spectra which showed that calcium caused the Trp residue to be in a less polar, more buried environment. In contrast to the other two pairs of IQ motifs, calcium increases the accessibility of the Trp in the 3–4IQ-CaM complex.

Thrombin Cleavage—It is known that CaM dissociates from one or more sites in the presence of calcium and the absence of exogenous CaM. From the spectroscopic results described above, we conclude that CaM remains bound to motifs, 1, 3, and 5, albeit in a different conformation than in the apo state. Limited proteolysis is a complementary technique to probe conformational changes in the IQ motifs that are spectroscopically silent.

IQ motifs 1, 2, 4, and 5 of murine myosin V contain a thrombin cleavage site, namely Arg-Gly of the consensus sequence. Note that the corresponding residues are Arg-Met in motif 3 and Arg-Arg in motif 6, and thus, these motifs cannot be cleaved by thrombin (Fig. 5). Cleavage of the IQ motif will only occur if the site is exposed by CaM dissociation or by a signifi-

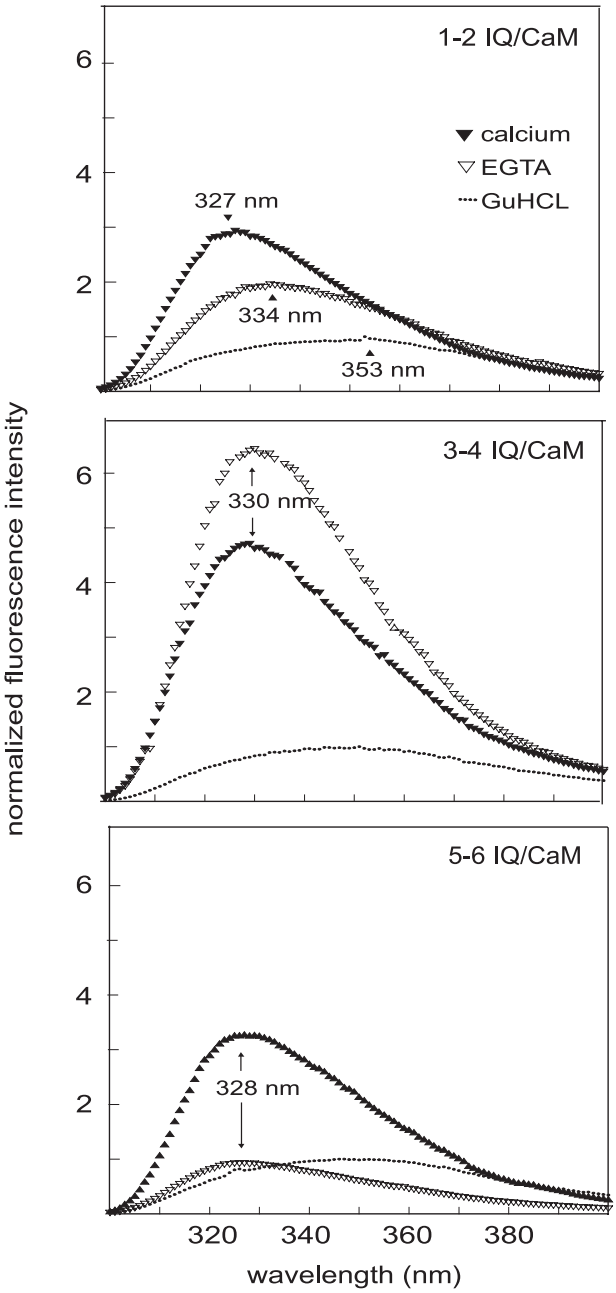

FIGURE 6. **Tryptophan fluorescence spectra of the CaM-IQ complexes.** The fluorescence spectra were recorded in the presence (*filled triangle*) or absence (*open triangle*) of calcium. The maximum of the spectrum obtained in the presence of guanidine hydrochloride was normalized to 1 for each complex (*dotted line*).

TABLE 1

Acrylamide quenching parameters of IQ-CaM complexes containing a single Trp

Emission peak maximum (λ_{max}) was determined from steady-state fluorescence spectrum. The same emission maximum was obtained after acrylamide quenching for the all IQ-CaM complexes. Dynamic (K_{SV}) and static (V) acrylamide quenching constants were calculated using the Stern-Volmer equation (see "Materials and Methods"). 1 mM EGTA or 100 μM $CaCl_2$ was used.

IQ-CaM complex	K_{sv} (M^{-1})		V (M^{-1})	
	EGTA	$CaCl_2$	EGTA	$CaCl_2$
	M^{-1}		M^{-1}	
1–2	3.95 ± 0.38	3.20 ± 0.53	1.11 ± 0.10	0.52 ± 0.23
3–4	3.50 ± 0.36	5.38 ± 0.32	0.28 ± 0.15	0.28 ± 0.10
5–6	3.65 ± 0.16	1.70 ± 0.09	~0	0.34 ± 0.05

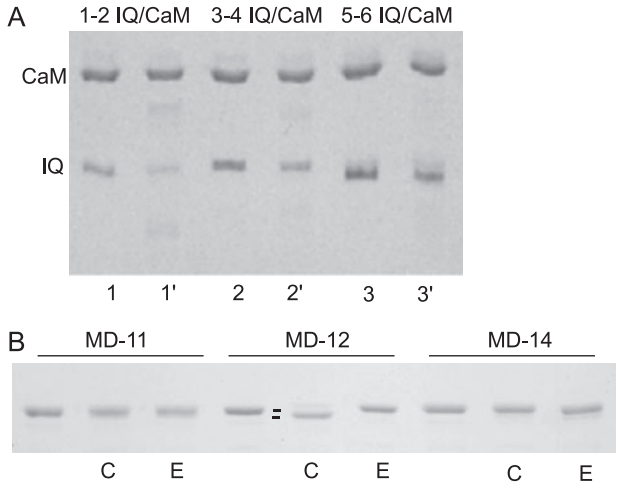

FIGURE 7. **Thrombin cleavage of IQ-CaM complexes.** *A*, pairs of IQ motifs were subjected to thrombin digestion in the presence of calcium. The only pair to show significant cleavage of the IQ motif peptide was the 1–2 IQ-CaM complex. Each pair of lanes shows undigested and then the digested sample. *B*, cleavage of MD-2IQ complexes with different pairs of IQ motifs after the motor domain, as indicated. Only the construct with IQ motifs 1,2 after the motor domain (*i.e.* the wild-type construct) was cleaved by thrombin. The MD-1,6 IQ construct was also not cleaved (data not shown). Each *triplet of lanes* shows undigested protein, thrombin digestion in the presence of calcium (*C*), and thrombin digestion in EGTA (*E*). *Dashes* indicate intact and cleaved positions.

cant reorganization of the bound CaM. Whether bound or free, CaM is not cleaved by thrombin. The only pair of IQ motifs to show cleavage of the IQ motif was the 1–2 IQ-CaM complex in the presence of calcium (Fig. 7*A*, *lane 1'*). Knowing from the spectroscopic data that CaM remains bound to site 1 in the presence of calcium, we infer that CaM can dissociate from, or significantly reorganize on IQ motif 2 in the presence of calcium.

To verify the results obtained with the peptide-CaM complexes, a wild-type and three mutant MD-2IQ constructs were expressed and subjected to thrombin cleavage. In each of these, the second IQ motif following the motor domain was replaced by sequences from either the first, fourth, or sixth IQ motif of the wild-type molecule (MD-11 IQ, MD-14 IQ, MD-16 IQ). The only one of these constructs to be cleaved by thrombin in the presence of calcium was the wild-type construct (MD-12 IQ), confirming the result with the peptides that site 2 is no longer protected from cleavage in the presence of calcium (Fig. 7*B*).

DISCUSSION

This study provides the first structural information on how calcium binding to CaM affects the actin-bound structure of myosin V. Calcium causes significant changes both in the disposition of the lever arm as well as propagated changes that extend into the motor domain. Several regions change in the motor domain upon calcium binding; loop 1 at the entrance to the active site becomes destabilized and rebinds in a different place, whereas loop 2 at the actin interface slightly changes position. The SH3 domain near the N terminus of myosin becomes destabilized, as does the region around the SH2 helix. In the lever arm, calcium changes the position of both CaMs, with the first CaM tilting up and sliding down, and the second CaM tilting in a different direction and moving down. The relative orientation between the two CaMs is also altered from that observed in the absence of calcium (see Fig. 3 and the supplemental movies). The lever arm conformation we observed is obtained with full actin decoration, where contacts between neighboring molecules occur. In the absence of these contacts it is possible that the neck conformation may be modified. Analysis of the electron microscopic data showed that the density for the second CaM in the presence of calcium is considerably less well defined than the CaM adjacent to the motor domain. The large AVID peak centered on the second CaM suggests partial occupancy, which is likely due to complete CaM dissociation from a subpopulation of molecules (Fig. 2, *blue*). We did not observe an extended conformation similar to that seen by Terrak *et al.* (31), in which only the C-lobe of a calmodulin-like light chain interacted with the IQ motif. This conformation was observed in the fourth IQ motif of a class V myosin from yeast. Our structural results are consistent with the proteolytic and spectroscopic studies presented here as well as earlier studies using different techniques, which suggest that calcium dissociates CaM from IQ motif 2 (5, 32–34).

Conformation of Bound Calcium-CaM—IQ motifs are unusual in that they have high affinity for CaM in the absence of calcium. The crystal structure of apoCaM bound to the first two IQ motifs of myosin V showed that the C-lobe of CaM is in a semi-open conformation that grips the first part of the IQ consensus motif (IQ*XXX*R), whereas the N-lobe is in a closed, non-gripping conformation that interacts more weakly with the second half of the IQ motif (G*XXX*R). Thus, it is the new semi-open conformation of the C-lobe that provides the major binding strength for the apoCaM-IQ complex. Unbound apoCaM, in contrast, would have both lobes in a closed, non-gripping conformation. The IQ motif, however, also has the necessary amphipathic character to bind calcium-CaM in a manner similar to many target peptides, with a basic surface on one side and a hydrophobic face on the other. Calcium binding would cause both lobes of CaM to adopt an open, gripping conformation, and both lobes would play similar roles in binding to the IQ target. The resolution of the electron microscopic reconstructions allowed us to show calcium-dependent changes in lever arm orientation and relative changes in orientation between the first and second CaMs, but it did not allow us to directly address the question of lobe conformation.

Fluorescence spectroscopy was used to detect conformational differences between the bound apoCaM and calcium-CaM states. In murine myosin V, only the odd numbered IQ motifs (1, 3, and 5) have a single Trp residue, whereas the even numbered motifs have no Trp. Thus, pairs of IQ motifs (1–2, 3–4, or 5–6) contain a single Trp that serves as a useful intrinsic

probe for CaM binding and conformation. The blue-shifted wavelength maxima of all three pairs of motifs compared with the unbound IQ motif is strong evidence that CaM is bound to IQ motifs 1, 3, and 5 both in the presence and absence of calcium (Fig. 6). The crystal structure of apoCaM 1–2 IQ shows that Trp is a major anchoring residue for the C-lobe in the apo state (Fig. 5*B*), and a single Trp residue is often found in many peptides that bind CaM in the presence of calcium (35).

When calcium was added to the bound apoCaM-IQ complex, IQ motifs 1 and 5 both showed an increase in fluorescence. These two motifs have Trp in the eighth position of the IQ motif (IQ*XXX*RG*WXX*R). Interestingly, the magnitude of the fluorescence in the 5–6 IQ motif in the absence of calcium was very low, the same as that observed with the unbound IQ peptide. The blue-shifted wavelength maximum of 328 nm, however, clearly indicates that the Trp is in a hydrophobic environment. How can these observations be resolved? It has been previously observed that Met residues, and much more effectively, selenomethionine, can quench Trp fluorescence (36). This tool was used to probe the binding of calcium-CaM to non-IQ target peptides. CaM has four Met residues in the C-lobe (Met-109, Met-124, Met-144, Met-145), three of which are within 10 Å of the Trp residue in the first motif in the apo state (13), and a similar situation is likely to exist in IQ motif 5. The significant quenching of Trp fluorescence in the fifth IQ motif, which is relieved by calcium binding, suggests that there is a significant calcium-dependent rearrangement of the C-lobe. The quenching phenomenon is highly distance-dependent and, thus, very sensitive to conformational changes (36). The observation that the fluorescence of the 1–2 IQ-CaM complex is quenched to a lesser extent than the 5–6 motif suggests that the orientation of the bound CaM varies from motif to motif, presumably as a result of sequence differences in the non-consensus residues. The apoCaM 1–2 IQ motif crystal structure showed that the variable residues in the IQ motif play a critical role in determining the precise structure of the bound CaM, which in turn affects how the consensus residues of different motifs interact with CaM (13). The 3–4 IQ motif is the only one to show an increase in fluorescence upon calcium binding, which likely reflects the fact that the Trp residue is in a different position of the IQ motif (IQ*XX*W*R*G*XXX*RG) compared with motifs 1 and 5 (IQ*XXX*RG*W*R). Acrylamide quenching data for all three pairs of motifs showed a lower quenching constant in the state that showed the highest fluorescence intensity, consistent with Trp being in a more buried, less solvent-exposed environment.

CaM Preferentially Dissociates from IQ Motif 2 in the Presence of Calcium—An unresolved issue has been the IQ motif from which CaM dissociates in the presence of calcium. Based on the current study and earlier work by us and others, we favor IQ motif 2 of murine myosin V as the site with the lowest affinity for CaM in the presence of calcium. Site 2 was first implicated from studies which showed that MD or MD-1IQ exhibited calcium-independent motility, whereas calcium abolished motility of MD-2IQ. The motility of MD-2IQ in calcium could be restored by the addition of exogenous CaM, suggesting that calcium-CaM can bind to IQ motif 2 but with a lower affinity than apoCaM (32). The fluorescence data shown here provide additional evidence that CaM remains bound to the first IQ motif in the presence of calcium. Only at very low protein concentrations would calcium-CaM be expected to dissociate from IQ motif 1 (K_d for binding was estimated as <30 nM (33)). The simplest explanation for our data is that CaM predominantly dissociates from site 2 in the presence of calcium and the absence of exogenous CaM. Thrombin cleavage of IQ motif 2 in the presence of calcium is also consistent with CaM dissociation, which allows cleavage between Arg-Gly, two of the consensus residues of the IQ motif. This cleavage was observed both in isolated pairs of IQ motifs as well as in constructs that contain the motor domain and various combinations of pairs of IQ motifs (Fig. 7).

Measurement of the affinity of CaM for single IQ motifs showed that the K_d for IQ motif 2 in the presence of calcium is 12.6 μM, whereas all the other motifs were <30 nM (33). An assumption is that single IQ motifs display similar properties to those that they have in the myosin lever arm where adjacent CaMs are present. These investigators further suggested that calcium causes CaM to interact with two adjacent IQ motifs, causing CaM dissociation because of formation of a high affinity "bridging" complex and not because of a calcium-dependent reduction in affinity of CaM for a particular motif. Our structural data provide no evidence for CaM forming a bridging complex in the 1–2 IQ motif pair when attached to the motor domain.

When myosin V purified from chick brain was digested with proteinase K in the presence of calcium, a subfragment that retained one CaM, and which could rebind a second CaM was formed (34). The authors suggested that CaM dissociated from and can reassociate with the second IQ motif. The fact that a similar conclusion was reached with whole myosin V and with the MD-2IQ construct used here, each using different techniques and approaches, lends strong support to the idea that results obtained with the truncated MD-2IQ construct are applicable to the native molecule. Another interesting finding in the study of Koide *et al.* (34) was that the IQ motif adjacent to the motor domain was occupied by CaM and not by a specific light chain. In contrast, constructs of chicken myosin V that have been crystallized were expressed with a specific light chain (LC1-sa) adjacent to the motor domain (37, 38). We have expressed and purified murine myosin V MD-1IQ with either CaM or LC1-sa at the first IQ motif, showing that the IQ motifs can somewhat promiscuously bind CaM-like proteins (data not shown).

It is not clear from the sequence of IQ motif 2 *per se* why it is the motif with the lowest affinity for CaM in the presence of calcium. Only a detailed structural analysis of the exact interactions will likely solve this issue. We have not ruled out the possibility that in the full-length neck, the position of the motif relative to the motor domain plays some role in determining the affinity for CaM by virtue of its interactions with the neighboring motifs.

Effect of Calcium on Myosin V Function—In the absence of calcium, myosin V adopts a folded, inactive conformation in which the cargo binding domain interacts with the motor domain near the active site (5–9). There are two pathways to unfold and activate the molecule; they are by binding cargo and

disrupting the head-tail interaction in the absence of calcium or by binding low concentrations of calcium. How can calcium cause activation when the site of head-tail interaction in the folded conformation does not appear to directly involve CaM? Based on the structural results described here, the observed change in lever arm orientation in the presence of calcium may be sufficient to disrupt the head-tail interaction. Thus, a direct interaction of the cargo binding domain with CaM in the folded state need not be invoked to explain the activating effect of calcium.

Once activated, higher calcium concentrations have an inhibitory effect on myosin V function; ensemble motility is inhibited, and processive runs are stopped (5, 10, 11). These effects are interpreted as due to dissociation of calcium-CaM from IQ motif 2. CaM dissociation effectively creates a compliant lever arm in which strain-dependent coordination of the two heads, necessary for processive motion, cannot occur. In ensemble measurements, motility can be restored by the addition of exogenous CaM because some motors at any given time will have a full complement of calcium-CaM bound to the IQ motifs (5). At the single molecule level, however, CaM dissociation terminates the processive run of a single motor (11). Although processive run length decreases with increasing calcium concentration, velocity remains constant, implying that the rate of ADP release is not affected by calcium once the motor is in an active state (11). In agreement, the V_{max} of the actin-activated ATPase activity of the MD-2IQ construct is not affected by calcium, again showing that ADP release *per se* is not affected by calcium (5). The ADP release rate is regulated, however, between the folded and the extended conformation of myosin V, which is a calcium-regulated process (11). The calcium-induced changes in activity of myosin V are, therefore, due to a combination of dissociation of bound CaM from IQ motif 2 and rearrangement of the bound CaM on other sites.

Acknowledgments—We thank Carol Bookwalter and Art Rovner for the data that generated Fig. 7B.

REFERENCES

1. Reck-Peterson, S. L., Provance, D. W., Jr., Mooseker, M. S., and Mercer, J. A. (2000) *Biochim. Biophys. Acta* **1496,** 36–51
2. Trybus, K. M. (2005) *Nat. Cell. Biol.* **7,** 854–856
3. Sellers, J. R., and Veigel, C. (2006) *Curr. Opin. Cell Biol.* **18,** 68–73
4. Wang, F., Chen, L., Arcucci, O., Harvey, E. V., Bowers, B., Xu, Y., Hammer, J. A., III, and Sellers, J. R. (2000) *J. Biol. Chem.* **275,** 4329–4335
5. Krementsov, D. N., Krementsova, E. B., and Trybus, K. M. (2004) *J. Cell Biol.* **164,** 877–886
6. Wang, F., Thirumurugan, K., Stafford, W. F., Hammer, J. A., III, Knight, P. J., and Sellers, J. R. (2004) *J. Biol. Chem.* **279,** 2333–2336
7. Li, X. D., Mabuchi, K., Ikebe, R., and Ikebe, M. (2004) *Biochem. Biophys. Res. Commun.* **315,** 538–545
8. Liu, J., Taylor, D. W., Krementsova, E. B., Trybus, K. M., and Taylor, K. A. (2006) *Nature* **442,** 208–211
9. Thirumurugan, K., Sakamoto, T., Hammer, J. A., III, Sellers, J. R., and Knight, P. J. (2006) *Nature* **442,** 212–215
10. Nguyen, H., and Higuchi, H. (2005) *Nat. Struct. Mol. Biol.* **12,** 127–132
11. Lu, H., Krementsova, E. B., and Trybus, K. M. (2006) *J. Biol. Chem.* **281,** 31987–31994
12. Volkmann, N., Liu, H., Hazelwood, L., Krementsova, E. B., Lowey, S., Trybus, K. M., and Hanein, D. (2005) *Mol. Cell* **19,** 595–605
13. Houdusse, A., Gaucher, J. F., Krementsova, E., Mui, S., Trybus, K. M., and Cohen, C. (2006) *Proc. Natl. Acad. Sci. U. S. A.* **103,** 19326–19331
14. Meador, W. E., Means, A. R., and Quiocho, F. A. (1992) *Science* **257,** 1251–1255
15. Kuboniwa, H., Tjandra, N., Grzesiek, S., Ren, H., Klee, C. B., and Bax, A. (1995) *Nat. Struct. Biol.* **2,** 768–776
16. Zhang, M., Tanaka, T., and Ikura, M. (1995) *Nat. Struct. Biol.* **2,** 758–767
17. Volkmann, N., Hanein, D., Ouyang, G., Trybus, K. M., DeRosier, D. J., and Lowey, S. (2000) *Nat. Struct. Biol.* **7,** 1147–1155
18. Owen, C. H., Morgan, D. G., and DeRosier, D. J. (1996) *J. Struct. Biol.* **116,** 167–175
19. Hanein, D., Matsudaira, P., and DeRosier, D. J. (1997) *J. Cell Biol.* **139,** 387–396
20. Egelman, E. H. (2000) *Ultramicroscopy* **85,** 225–234
21. Ludtke, S. J., Baldwin, P. R., and Chiu, W. (1999) *J. Struct. Biol.* **128,** 82–97
22. Volkmann, N., and Hanein, D. (1999) *J. Struct. Biol.* **125,** 176–184
23. Volkmann, N., and Hanein, D. (2003) *Methods Enzymol.* **374,** 204–225
24. Holmes, K. C., Angert, I., Kull, F. J., Jahn, W., and Schroder, R. R. (2003) *Nature* **425,** 423–427
25. Hanein, D., and DeRosier, D. (1999) *Ultramicroscopy* **76,** 233–238
26. Volkmann, N. (2002) *J. Struct. Biol.* **138,** 123–129
27. Murshudov, G. N., Vagin, A. A., and Dodson, E. J. (1997) *Acta Crystallogr. D Biol. Crystallogr.* **53,** 240–255
28. Rost, L. E., Hanein, D., and DeRosier, D. J. (1998) *Ultramicroscopy* **72,** 187–197
29. Eftink, M. R., and Ghiron, C. A. (1976) *Biochemistry* **15,** 672–680
30. Volkmann, N., Ouyang, G., Trybus, K. M., DeRosier, D. J., Lowey, S., and Hanein, D. (2003) *Proc. Natl. Acad. Sci. U. S. A.* **100,** 3227–3232
31. Terrak, M., Wu, G., Stafford, W. F., Lu, R. C., and Dominguez, R. (2003) *EMBO J.* **22,** 362–371
32. Trybus, K. M., Krementsova, E., and Freyzon, Y. (1999) *J. Biol. Chem.* **274,** 27448–27456
33. Martin, S. R., and Bayley, P. M. (2004) *FEBS Lett.* **567,** 166–170
34. Koide, H., Kinoshita, T., Tanaka, Y., Tanaka, S., Nagura, N., Meyer zu Horste, G., Miyagi, A., and Ando, T. (2006) *Biochemistry* **45,** 11598–11604
35. Crivici, A., and Ikura, M. (1995) *Annu. Rev. Biophys. Biomol. Struct.* **24,** 85–116
36. Yuan, T., Weljie, A. M., and Vogel, H. J. (1998) *Biochemistry* **37,** 3187–3195
37. Coureux, P. D., Wells, A. L., Menetrey, J., Yengo, C. M., Morris, C. A., Sweeney, H. L., and Houdusse, A. (2003) *Nature* **425,** 419–423
38. Coureux, P. D., Sweeney, H. L., and Houdusse, A. (2004) *EMBO J.* **23,** 4527–4537